Water Research 169 (2020) 115286

Contents lists available at ScienceDirect

Water Research

journal homepage: www.elsevier.com/locate/watres

Significance of the micropores electro-sorption resistance in capacitive deionization systems

Yasamin Salamat, Carlos H. Hidrovo*

Mechanical and Industrial Engineering Department, Northeastern University, 334 Snell Engineering Center, 360 Huntington Ave, Boston, MA, 02115, USA

ARTICLE INFO

Article history:
Received 16 July 2019
Received in revised form
12 October 2019
Accepted 5 November 2019
Available online 6 November 2019

Keywords:
Capacitive deionization
Dynamic ion adsorption theory
Adsorption resistance
Energetic efficiency
Water desalination

ABSTRACT

Capacitive Deionization (CDI) is an emerging technology representing a potential alternative to the common, energy-intensive desalination methods for low salinity water streams. In CDI an electrical field is applied to separate ionic species from aqueous solutions and electro-adsorb them into a highly porous material. CDI is a complex multi-scale system which requires robust mathematical models to closely describe its performance. Here, a dynamic two-dimensional model is developed coupling the diffusion and advection of the species in the bulk solution with their diffusion and electro-sorption in the porous electrodes. In this model, the adsorption/desorption resistance between the micropores and macropores along with variable non-electrostatic attractive forces in the micropores are also incorporated. The proposed theory is validated against experiments using a circular CDI cell operating under various conditions, where different transport mechanisms are limiting the total ion removal process. Performance of the CDI systems is also evaluated using inclusive figures of merit. The obtained results accentuate the significant effect of the rate-limited transfer of the ionic species from the macropores into the micropores, especially in systems subject to severe ion starvation, where neglecting this electro-sorption resistance leads to up to 50% and 210% overestimation of the energy efficiency and overall desalination performance, respectively. Furthermore, although the commonly used transport theory describing CDI fails to capture the dynamics of the systems at low initial concentration and high adsorption capacity by assuming fast electro-sorption without any resistance, the presented theory closely models the transport mechanisms in such systems. Moreover, we experimentally and numerically demonstrate a trade-off between the energetic and desalination performance in systems with low and high mass Péclet number.

1. Introduction

Secure and sustainable water resources are essential for social and economic development, ecological health, and humans' well-being. However, satisfying the unprecedented water demands of the ever-growing population of the planet with the significantly limited available resources is one of the major challenges of our era. Due to its abundance, brackish groundwater (with total dissolved solids (TDS) of 1–10 mg/ml) has the potential to play an important role in this scenario. In the US alone, the total amount of brackish groundwater available is about 800 times more than that of the saline groundwater and 35 times more than the fresh groundwater withdrawn nationwide, each year (Stanton and P.B. 2017). Moreover, the theoretical minimum energy required to desalinate brackish water is less than that needed for higher salinity water (Elimelech and Phillip, 2011). Hence, consuming a small fraction of this valuable water resource can alleviate the fresh water shortage crisis in many water-scarce regions, rendering efficient means of water desalination of paramount importance.

Capacitive Deionization (CDI) is a relatively new technology which has the potential to serve as a highly efficient and low-cost alternative for low salinity water desalination. In CDI, a low DC potential difference (1–1.2 V) is used to apply an electric field to remove ionic species from water streams and electrostatically adsorb them into the Electrical Double Layers (EDLs) formed at the surface of a highly porous material (Anderson et al., 2010; Oren, 2008; Suss et al., 2015; Xu et al., 2008). Extraction of these ions lowers the solution concentration at the exit. The electrodes can then be discharged and regenerated by desorbing the electro-adsorbed ions. Over the past decade, the CDI technology has

* Corresponding author.
E-mail address: hidrovo@neu.edu (C.H. Hidrovo).

https://doi.org/10.1016/j.watres.2019.115286
0043-1354/

greatly expanded by the introduction of various CDI configurations (Gao et al., 2015; Hatzell et al., 2015; Omosebi et al., 2017; Smith and Dmello, 2016; Tang et al., 2019), physical and chemical modification of the electrodes (Arulrajan et al., 2019; Bhat et al., 2019; Gao et al., 2016; Liu et al., 2015; Oyarzun et al., 2018; Wu et al., 2015), optimization of the operating conditions (Cohen et al., 2015, Demirer et al., 2013, Ramachandran et al., 2019b, Salamat et al., 2016a, b, Shang et al., 2017), standardization of performance metrics (Hand et al., 2019; Hawks et al. 2018a, 2019; Salamat and Hidrovo, 2018), and theoretical analysis of CDI systems (Dykstra et al., 2017; Hemmatifar et al., 2017; Qu et al., 2018; Ramachandran et al., 2018).

CDI is a complex system comprised of several highly coupled transport mechanisms taking place at different length and time scales. Hence, developing a comprehensive theoretical framework validated by experimental data is vital to understand the underlying physics and improve the performance of this technology. Based on the concept of the Donnan equilibrium, the modified Donnan (mD) theory was introduced by Biesheuvel et al. which is suitable for the two-tier pore size assumption (micropores and macropores with dimensions of <2 nm and >50 nm, respectively) in porous carbon electrodes (Biesheuvel et al. 2011a, 2011b). This theory has been extensively used to develop one- and two-dimensional models describing the transport mechanisms and salt adsorption in CDI systems (Biesheuvel et al., 2011a; Dykstra et al., 2016b; Guyes et al., 2017; He et al., 2018; Hemmatifar et al., 2015; Porada et al., 2013; Suss et al., 2014). In all the theories based on the mD model, highly overlapped EDLs are assumed in the micropores while their extension in the macropores is being neglected compared to the dimensions of these pores. This allows for the premise of uniform concentration of species and electric potential in the micropores and electroneutrality in the macropores.

Analytical solutions have also been developed using simple dynamic response models (Hawks et al., 2018a; Jande and Kim, 2013). However, neglecting the formation of the EDLs and the associated dynamics, these models are not able to fully capture the physics of CDI.

So far, all the models studying the underlying physics of CDI have overlooked a possible resistance for the adsorption/desorption of species from the macropores into the micropores and vice versa, assuming that this motion happens instantly. However, as with any other transport mechanism, there should be a resistance to this motion. Although a few studies have referred to this transport resistance, to the best of our knowledge, no work has incorporated it in the theoretical analysis (Porada et al., 2013; Suss et al., 2015). Even though Mubita et al. included an equation taking into account the rate of transport between the micro- and macropores, they considered a high kinetic rate constant, implying that the ion transport between the macro- and micropores is at equilibrium and no rate limitation exists for this transfer (Mubita et al., 2018).

Here, the implemented 2D model in our previous work (Salamat and Hidrovo, 2018) is further extended to incorporate the improved modified Donnan (i-mD) theory (Biesheuvel et al., 2014). Moreover, rather than assuming fast ion adsorption and desorption from the macropores into the micropores and vice versa, the model is modified to capture the transport resistance for this motion using a formulation akin to the Butler-Volmer equation utilized for describing the charge transfer rate in redox reactions. The numerical results are then validated with experimental data from desalination cases with different characteristic dimensionless numbers. The desalination and energetic performance of these systems are also evaluated using the previously proposed figures of merit (Salamat and Hidrovo, 2018).

2. Theory

In this work, the Nernst-Planck equation is used to describe the transport of the charged species in the main channel:

$$p_s\frac{\partial c_i}{\partial t} = -\nabla.\left(c_i u - p_s D_i \nabla c_i - p_s\frac{z_i D_i}{V_T}c_i\nabla\varphi\right) \tag{1}$$

where c_i, D_i, and z_i are the concentration, diffusion coefficient, and valence of the species i, respectively, and p_s is the porosity of the spacer. u and φ are associated with the velocity vector and electric potential at each location, respectively. V_T refers to the thermal voltage, calculated as k_BT/e, where k_B is the Boltzmann constant, T is the absolute temperature, and e is the elementary electric charge. Assuming equal diffusion coefficients and based on the electroneutrality approximation, by adding and subtracting Equation (1) for $i = \pm 1$ (binary salt with monovalent ions), the transport of the species in the main channel can be expressed as:

$$p_s\frac{\partial c}{\partial t} = -\nabla.(cu - p_s D\nabla c) \tag{2}$$

$$\nabla.(c\nabla\varphi) = 0 \tag{3}$$

In these set of equations, c and D are used as the concentration of the salt (which is equal to that of both positive and negative ions based on the above assumptions, i.e. $c_+ = c_- = c$) and the diffusivity of the species in the main channel, respectively. Equation can also be used to explain the motion of the species in the macropores of the porous electrode by introducing an additional term to include the adsorption/desorption of the ions from the macropores into the micropores and vice versa:

$$p_{Ma}\frac{\partial c_i}{\partial t} = -\nabla.\left(c_i u_e - D_{i,e}\nabla c_i - \frac{z_i D_{i,e}}{V_T}c_i\nabla\varphi\right) - j_{Ma-mi,i} \tag{4}$$

In the above equation, p_{Ma} stands for the porosity of the macropores and the term $j_{Ma\text{-}mi,i}$ refers to the rate of concentration change in the macropores due to the rate-limited transfer of species i between the macropores and micropores. Effective diffusivity of the species in the porous electrodes $D_{i,e}$ can be obtained as $p_{Ma}D_i/\tau$, where τ is the tortuosity of the structure. We apply the electroneutrality assumption in the macropores and assume no flow in the porous structure. Therefore, by adding and subtracting Equation for both positive and negative ions, the transport equations can be written as:

$$p_{Ma}\frac{\partial c}{\partial t} = \frac{p_{Ma}}{\tau}D\nabla^2 c - \left(\frac{j_{Ma-mi,+} + j_{Ma-mi,-}}{2}\right) \tag{5}$$

$$\frac{p_{Ma}}{\tau}\frac{D}{V_T}\nabla(c\nabla\varphi) = \left(\frac{j_{Ma-mi,+} - j_{Ma-mi,-}}{2}\right) \tag{6}$$

The adsorption and desorption rate of positively and negatively charged species can be related to the rate of change in their concentration in the micropores $c_{mi,i}$ as:

$$p_{mi}\frac{\partial c_{mi,i}}{\partial t} = j_{Ma-mi,i} \tag{7}$$

where p_{mi} is the porosity of the micropores.

Here, the i-mD model is used to describe the adsorption and desorption of the ionic species in the EDLs formed in the micropores of the electrodes (Biesheuvel et al., 2014; Dykstra et al., 2016b; Kim et al., 2015b). In this model, the micropores which include the solution and the electrode's surface are also assumed to

be electroneutral. Therefore, the ionic charge density in the solution, q_{ion}, and the electronic charge density in the electrode's matrix, q_{elec}, balance each other in the micropores. The ionic charge and the potential difference in the micropores can then be related according to:

$$-Fq_{ion} = C_s \Delta\varphi_{mi} \tag{8}$$

In this equation, F is the Faraday constant (9.6485×10^4 C/mol) and q_{ion} (with units of moles per micropore volume) can be calculated as $c_{mi,+} - c_{mi,-}$. C_s is the volumetric specific capacitance of the electrode and is expressed in Farads per unit volume of the micropores and $\Delta\varphi_{mi}$ is the potential difference between the surface of the charged electrode and the micropore.

As mentioned earlier, all the mathematical models developed so far for CDI assume instantaneous adsorption/desorption of ions into/from the micropores, and to the best of our knowledge, no studies have fully explored the effects of electro-sorption resistance in CDI cells. To incorporate this resistance in our model, the transport of ions from the macropores into the micropores can be modeled in a similar fashion to the transfer of electrons in redox reactions (although the redox reactions per se are not considered in this work). Assuming a single step, first order redox reaction, anodic and cathodic reactions both occur simultaneously at each electrode, but in the opposite directions. In electrochemical kinetics, the Butler-Volmer equation is used to describe the charge transfer rate, or in other words, the resistance to the charge transfer in the electrode reactions (Newman and Thomas-Alyea, 2012; Prentice, 1991). The general form of this equation can be written as:

$$j = Fk_0 \left[c^s_{red} \exp\left(\alpha \frac{E - E^0}{V_T}\right) - c^s_{ox} \exp(-(1-\alpha)\frac{E - E^0}{V_T}\right] \tag{9}$$

where j is the current density at the electrode, k_0 is the rate constant, α is the transfer coefficient, and E and E^0 are the applied and equilibrium potentials, respectively. c^s_{red} and c^s_{ox} refer to the concentration of the reduced and oxidized species at the surface of the electrode, respectively. To incorporate the resistance to the transfer of ions between the macro- and micropore in CDI, an analogy can be drawn between this transport and the transfer of electrons in redox reactions. In the context of CDI too, two processes affect the adsorption (desorption) of the counter-ions (co-ions) in two opposite directions (see Fig. 1). First is the electro-adsorption of the counter-ions into the micropores due to the electrostatic forces, and second is their diffusion from the micropores with higher counter-ion concentration into the macropores with lower concentration. Co-ions are also affected by the same processes, although in the reverse direction: electro-desorption from the micropores and diffusion from the macropores into the micropores. Nevertheless, it should be noted that in the two-tier pore size models based on the mD theory, including the one implemented here, only the micropores and macropores are being considered. Hence, the definition of a physical length scale for the diffusion of the ions from the micropores into the macropores and vice versa is not trivial. Therefore, employing the explained analogy, and as suggested by the previously discussed studies, an explicit expression similar to the Butler-Volmer equation used for describing the rate of the redox reactions taking place in electrochemical cells is employed to include the transport resistance between the micro- and macropores (Mubita et al., 2018; Porada et al., 2013; Suss et al., 2015):

$$j_{Ma-mi,i} = k \left[c_i \exp\left[\left(\alpha\left(-\frac{z_i \Delta\Phi_D}{V_T} + \frac{\mu_{att}}{k_B T}\right)\right) - c_{mi,i} \exp(1-\alpha).\left(\frac{z_i \Delta\Phi_D}{V_T} - \frac{\mu_{att}}{k_B T}\right)\right]\right] \tag{10}$$

In the above equation, k is the transfer rate constant (1/s) and is assumed to be the same for both anions and cations. α is set to 0.5 here, which is the typical assumption in the electrochemical studies. In the i-mD model, $(\Delta\Phi_D - \mu_{att}/e)$ refers to the total potential difference (in volts) between the micro- and macropores. $\Delta\Phi_D$ is the donnan potential, the electrostatic potential difference, and μ_{att}/e accounts for the non-electrostatic potential difference, where μ_{att} stands for the non-electrostatic adsorption energy of ions (in k_BT). This non-electrostatic adsorption term has been added to the mD-based theories to describe the experimentally observed decrease in the concentration of the inlet solution in CDI systems using porous carbon electrodes prior to applying any electric voltage (Biesheuvel et al. 2012, 2014; Kastening and Heins, 2005; Porada et al., 2013). For the large values of the rate constant k, the transfer of the ions between the macropores and micropores can be considered at equilibrium (i.e. no resistance exists for the transfer of the species between the macro- and micropores). This leads the above equation to reduce to the familiar Boltzmann distribution ($c_{mi,i} = c_i exp(-z_i \Delta\phi_D/V_T + \mu_{att}/k_BT)$) used in the mD-based models for describing the CDI process.

The main deviation of the i-mD from the standard version of the mD model is that in the former, μ_{att} is not a constant value and is indeed a function of the ionic concentration in the micropores. In other words:

$$\mu_{att} = \frac{E}{c_{mi,+} + c_{mi,-}} \tag{11}$$

where E is the micropore ion-correlation energy and is associated with the attractive Coulomb energy between an ion and its image charge in the carbon matrix (in units of $k_BT.mol/m^3$). This modification stems from the unrealistic estimation of the mD model for the salt adsorption of uncharged carbon electrodes in contact with solutions with a broad range of initial concentrations (Biesheuvel et al., 2014; He et al., 2018).

The net total electric potential available to the cell, φ_t, is calculates as:

$$\varphi_t = \varphi_{in} - IR_{ext} \tag{12}$$

φ_{in} is the external potential difference applied through the power supply and R_{ext} refers to all the external setup (the wires, the current collectors, and the main channel ionic solution) and the contact resistances. The interfacial capacitance of the current collectors

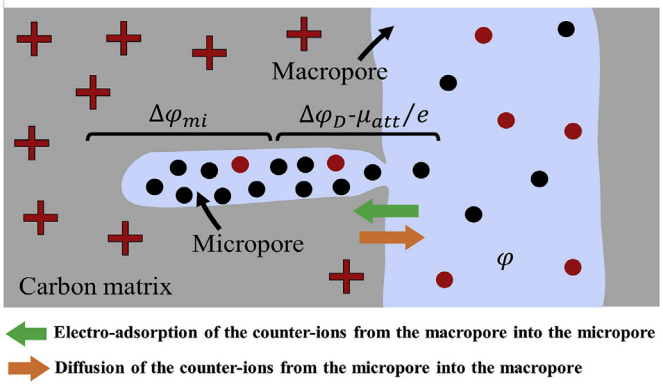

Fig. 1. Schematic illustration of the two mechanisms competing in the transfer of the ionic species between the macropores and micropores. For simplicity, the arrows here only refer to these mechanisms involved in the transport of the counter-ions between the micro- and macropores.

and the resistance in the matrix of the porous electrodes are neglected in these set of equations. I is the external electric current of the system and in the absence of unfavorable Faradaic reactions, can be calculated based on the electromigration of the ionic species through the interface of the electrode and the bulk flow (see Equation (6)):

$$I = \int p_{Ma} \frac{D}{\tau} \frac{F}{V_T} (2c) \frac{\partial \varphi}{\partial n} dA \tag{13}$$

In the above equation, n is the direction normal to the interface of the electrode and the main channel. Eventually, assuming symmetry with respect to the flow axis, the electric potentials in each electrode can be balanced as:

$$\frac{\varphi_t}{2} = \Delta\varphi_{mi} + \Delta\varphi_D + \varphi \tag{14}$$

It should be noted that in this model, we assume zero net chemical charge at the surface of the electrodes and therefore the potential at the point of zero charge (φ_{pzc}) is set to zero. Further information on the experimental validation of this assumption are provided in the subsequent sections.

While Equations (2) and (3) are used to model the transport in the main channel, Equations (1) and (5)–(8)0-14 are employed to describe the ionic motion within the porous electrodes.

As explained in our previous work, three timescales are associated with the transport mechanisms taking place in CDI units (Salamat and Hidrovo, 2018). The electro-diffusion timescale which is related to the combined diffusion and electro-sorption of species in the porous structure is defined as:

$$t_{elec-diff} = \frac{C_s L_e^2 \tau^2 p_{mi}}{D c_0 p_{Ma}} \frac{V_T}{2F} \tag{15}$$

where, c_0 is the initial concentration in the system and L_e is the thickness of the electrodes. The motion of the species in the bulk flow of the flow-between CDI (fbCDI) unit can be characterized through the bulk diffusion and bulk advection timescales. $t_{bulk\text{-}diff}$ and $t_{bulk\text{-}adv}$ can be calculated as L_g^2/D and Vol/Q, respectively. L_g, Vol, and Q are the gap distance between the electrodes, the volume of the cell, and the flow rate of the inlet solution, respectively. Here, we have to clarify that as discussed in our previous work, these timescales are described based on the classic mD theory, where electro-sorption is assumed to be infinitely fast without any resistance (Salamat and Hidrovo, 2018). In that study and also the work presented here, the electro-diffusion time constant is defined based on the diffusion resistance of the ions within the macropores and the adsorption capacity of the micropores, similar to a RC timescale. In other words, the electro-diffusion time constant does not consider the micro-to macropore transfer resistance. In this study, we also adhere to our previous framework (where we used classic mD theory as a baseline) and use the same terminology for the time constants.

Three non-dimensional parameters can be defined to compare these time constants:

1) Mass Péclet number, $Pe_m = t_{bulk\text{-}diff}/t_{bulk\text{-}adv}$, 2) Modified Damköhler number, $Da = t_{bulk\text{-}adv}/t_{elec\text{-}diff}$, and 3) Modified second Damköhler number, $Da_{II} = t_{bulk\text{-}diff}/t_{elec\text{-}diff}$. Standard Damköhler numbers are normally used to compare chemical reactions rates to the rate of advection or diffusion in a system. Although we assume no chemical reaction in the CDI unit, here we utilize the concept of the Damköhler numbers to compare the charging rate of the electrodes to the transport rate of the ions in the main channel, namely the bulk advection and bulk diffusion.

To validate the discussed model in this work, 7 distinct cases with different time constants are experimentally and numerically tested. More details on the conducted experiments are provided next.

3. Material and Methods

3.1. CDI validation experiments

Table 1 shows the characteristic non-dimensional parameters associated with the analyzed cases. It should be noted that to validate the developed model in this work, rather than focusing on one operational parameter at a time (for example, the applied potential difference or the inlet concentration), we use several desalination cases with different transport timescales and non-dimensional numbers. This approach is adopted to emphasize the importance of the characteristic time constants ($t_{bulk\text{-}adv}$, $t_{bulk\text{-}diff}$, and $t_{elec\text{-}diff}$) in CDI units and the ability of the proposed model to describe the performance of systems operating under different transport timescales. As discussed in our previous work, the transport timescales in the main channel and the electrodes and the associated non-dimensional numbers dictate the temporal behavior of the concentration at the outlet of CDI cells, as well as their desalination and energetic performance (Salamat and Hidrovo, 2018). In this work, 6 CDI cases are investigated in which two of the main transport mechanisms have the same order of magnitude time constant, while the third mechanism is about one order of magnitude faster or slower. Furthermore, the case where all the three transport phenomena have timescales of the same order is also investigated. To be more specific, in the first three cases, one transport mechanism is limiting the entire charging process (i.e. is the slowest one). In the 4th case, all the main salt transport mechanisms take place simultaneously in the bulk and electrodes. And in the last three cases, two mechanisms are simultaneously limiting the salt removal process (with the same order of magnitude time constants) while the third one is faster than these two mechanisms.

3.2. Experimental methods and model parameters derivation

To achieve the targeted non-dimensional numbers, the initial concentration, flow rate, and the gap distance are adjusted in the numerical and experimental tests. Flow rates range from 0.18 to 14 ml/min and the initial concentrations and the gap distances vary from 1 to 8 mM and from 0.8 mm to 3.2 mm, respectively. Experiments are conducted in a circular fbCDI unit, shown in Fig. S1 in the Supplementary Information, Section S1. Circular activated carbon electrodes with a diameter of 96 mm, average thickness of 238 μm, and mass of 0.75 gr (Material and Methods LLC., USA) and Titanium sheets with a thickness of 0.1 mm (MTI Corp., USA) serve as the porous material and current collector, respectively. To avoid electrical contact between the two sides of the unit, Polyester plastic mesh disks (McMaster-Carr, USA) with different thicknesses and openings are used. It is worth mentioning that, as shown in previous studies, performance of CDI cells is subject to degradation

Table 1
Characteristic timescales of the desalination cases which are experimentally and numerically tested here.

Case number	Characteristic timescale and non-dimensional numbers
Case 1	$t_{bulk\text{-}adv} \sim t_{bulk\text{-}diff} \ll t_{elec\text{-}diff}$: $Pe_m = 1.7$, $Da = 0.2$, $Da_{II} = 0.3$
Case 2	$t_{elec\text{-}diff} \sim t_{bulk\text{-}diff} \ll t_{bulk\text{-}adv}$: $Pe_m = 0.1$, $Da = 8.6$, $Da_{II} = 0.8$
Case 3	$t_{elec\text{-}diff} \sim t_{bulk\text{-}adv} \ll t_{bulk\text{-}diff}$: $Pe_m = 8.9$, $Da = 1.4$, $Da_{II} = 12.3$
Case 4	$t_{bulk\text{-}diff} \sim t_{bulk\text{-}adv} \sim t_{elec\text{-}diff}$: $Pe_m = 1.9$, $Da = 0.8$, $Da_{II} = 1.5$
Case 5	$t_{elec\text{-}diff} \ll t_{bulk\text{-}diff} \sim t_{bulk\text{-}adv}$: $Pe_m = 2.5$, $Da = 11$, $Da_{II} = 28.4$
Case 6	$t_{bulk\text{-}adv} \ll t_{bulk\text{-}diff} \sim t_{elec\text{-}diff}$: $Pe_m = 7.5$, $Da = 0.1$, $Da_{II} = 0.9$
Case 7	$t_{bulk\text{-}diff} \ll t_{bulk\text{-}adv} \sim t_{elec\text{-}diff}$: $Pe_m = 0.06$, $Da = 7$, $Da_{II} = 0.4$

under prolonged experiments (Gao et al., 2015; Omosebi et al., 2014; Zhang et al., 2018). The total duration of the experiments in this work differ from case to case, ranging from 1 to 7 days, as it depends on the characteristic transport timescales of each case. To avoid any degradation effect, a new and unused pair of electrodes is used for each case, and no evident performance decline is observed over the course of the experiments.

Fig. S2 illustrates the experimental setup used in this work. A potentiostat (ModuLab, Solartron analytical, USA) is utilized to apply 1 V for charging and 0 V for discharging the electrodes. The conductivity of the effluent is measured via a flow-through conductivity sensor (ET917, eDAQ, Australia) and is corrected for temperature changes using a J-type thermocouple located at the exit of the cell. The flow rate is also measured and recorded using a flow meter (SLS-1500, Sensirion, Switzerland). NaCl solutions are used as the inlet reservoir, the concentration of which are adjusted by using a 5 M solution (Sigma Aldrich, USA) and DI water. To remove the dissolved oxygen, the inlet solution is degassed in a vacuum chamber for 12 h before each experiment. The pH of the inlet reservoir is then measured using a pH probe (PH BTA, Vernier, USA), having the value of 6.98 ± 0.02. Additionally, prior to each experiment, the electrodes are presoaked in DI water to ensure that the pores are fully wetted. Several successive charge/discharge cycles are conducted for each case to make sure that the system has reached the dynamic equilibrium state (where the amount of salt adsorbed during desalination is equal to the amount of salt desorbed during regeneration).

There are several parameters associated with each experiment which need to be input in the model to correlate the experimental data with the numerical results. Cyclic Voltammetry (CV) is used to estimate the electrode's micropore capacitances, and the external resistance of the setup for each case is extracted utilizing Electrochemical Impedance Spectroscopy (EIS). The assumptions of zero point of charge (φ_{pzc}) and zero net chemical surface charge are also validated here. For this purpose, we use 200 ml of degassed 4 mM NaCl solution and soak one carbon electrode in it overnight. The pH of the solution before and after the submergence of the electrode is measured. The presence of different chemical surface groups changes the concentration of H^+ and OH^- and consequently, the pH of the solution due to different surface interactions at the surface of the carbon electrode (Gao et al. 2017, 2019; Hemmatifar et al., 2017). Recorded values of pH demonstrate negligible alteration in the pH value, from 6.5 before the insertion to the almost neutral value of 7.3 after the insertion. This verifies our assumption of zero φ_{pzc} and zero net chemical charge at the surface of the electrodes.

We refer the reader to the Supplementary Information document, Section S3 for further details on the parameter settings of the model. These settings result in only two main parameters to be fitted in our model: the ion-correlation energy E and the rate constant k, which are extracted from the experimental results of the equilibrium state and temporal concentration profile of the effluent in different desalination cases.

3.3. Performance evaluation of CDI tests

In addition to the effluent concentration profile of the CDI tests, the salt adsorption and the electronic charge transferred to the electrodes are calculated by the following equations, and used to evaluate the effectivity of the proposed model:

$$\delta = \frac{M_w \int_0^t (c_{out} - c_0) Q dt^*}{m_e} \tag{16}$$

$$q = \frac{\int_0^t I_{net} dt^*}{m_e} \tag{17}$$

δ is the salt adsorption and q is the electronic charge transferred to the electrodes (both per mass of the electrodes). M_w is the molar mass of the salt and m_e is the total mass of the used electrodes. $I_{net}(t)$ is the net current and is calculated as $I(t) - I_{leak}$ where $I(t)$ is the measured electrical current I_{leak} refers to the non-zero residual electrical current in the system long after the equilibrium is reached, which is usually attributed to the unfavorable parasitic reactions taking place at the surface of the electrodes (Hatzell et al., 2014; Hemmatifar et al., 2016; Shang et al., 2017).

The charge efficiency Λ of each case, defined as the ratio of the moles of salt removed to the moles of charge transferred to the electrodes, is also calculated from the experimental and numerical data using the following equation:

$$\Lambda = \frac{F\delta}{M_w q} \tag{18}$$

To further compare the output of the CDI cells predicted by the model with the experimental data, desalination and energetic performances of the analyzed cases are investigated. The desalination performance is evaluated using the *Ultimate Desalination Throughput (UDT)* defined as (Salamat and Hidrovo, 2018):

$$UDT = \frac{c_0 - c_{ave}}{c_0}((c_0 - c_{ave})Q)(t_{desal}Q) \tag{19}$$

c_{ave} is the average concentration of the effluent and is calculated as $c_{ave} = \frac{1}{t}\int_0^t c(t^*)dt^*$, and t_{desal} refers to the total desalination time. Here we use the average concentration as the performance evaluation point as it represents the final concentration of the collected treated water at the end of the desalination stage. The first term in the right-hand side of Equation (19) computes the desalination percentage in the system, and the second and the third terms determine the average rate of salt removal from the bulk solution and the total volume of the desalinated water, respectively. The significance of this figure of merit is that it combines three characteristics of a desirable desalination system, i.e. low average concentration of the effluent and fast ion adsorption from large volumes of the inlet stream. In addition, it represents the processing rate, which is equal to the rate at which the inlet water is being processed, times the amount of salt adsorbed.

To make a thorough assessment of the overall performance of a CDI unit, the performance of the regeneration process should also be considered. For that purpose, the *Overall Desalination and Regeneration Performance (ODRP)* is defined and calculated as:

$$ODRP = UDT\frac{WR}{t_{total}} \tag{20}$$

WR is the water recovery ratio and is defined as the ratio of the desalinated volume to the total volume of the initial solution and t_{total} is the total duration of the process (desalination and regeneration). This metric states that a favorable CDI desalination unit should at the same time incorporate high values of *UDT* (i.e. better adsorption performance) and high water recovery ratio over a shorter total processing time span.

Moreover, the energetic performances of the numerically and experimentally investigated cases are compared against each other. The thermodynamic efficiency of both sets of data is calculated as:

$$\eta = \frac{W_{rev}}{E_{in}} \tag{21}$$

W_{rev} is the theoretical minimum energy required to desalinate a given solution to the desired concentration and divide the solution into two desalinated and concentrated parts. This value is independent of the desalination method and can be calculated through the Gibbs free energy as (Bejan 2016; Biesheuvel, 2009; Hemmatifar et al., 2018):

$$W_{rev} = 2V_d\left(\frac{c_0}{WR}\ln\frac{c_0 - WR.c_d}{c_0(1-WR)} - c_d\ln\frac{c_0 - WR.c_d}{c_d(1-WR)}\right)RT \tag{22}$$

R is the universal gas constant and V_d and c_d are the volume and final concentration of the desalinated solution, respectively. E_{in} in Equation (21) is the actual electrical energy input during the desalination step (assuming zero energy recovery) and is obtained as:

$$E_{in}(t) = \int_0^t I_{net}(t^*)\varphi_{in}dt^* \tag{23}$$

φ_{in} refers to the external potential difference applied through the power supply.

To further accentuate the importance of including the micro-macropore transfer resistance in the mathematical model, we also compare the results obtained here with the numerical data from the 2D model with fast adsorption/desorption processes (classic i-mD with no electro-sorption resistance).

4. Results and discussion

4.1. Parameters extraction

CV and EIS data obtained in this work are depicted in Fig. S3 and Fig. S4, respectively. The experimental operational conditions and the model parameter settings for each of the mentioned cases are listed in the Supplementary Information document, section S4. We adopt the recommended approach of Hawks et al. for reporting these parameters and include the separation report of each case in this work (Hawks et al., 2018b).

Salt adsorption δ, charge q, and charge efficiency Λ at equilibrium do not depend on the transfer rate between the macropores and micropores. Therefore, these parameters can be evaluated to find the value for the micropore ion-correlation energy E which results in the best fit and minimum error between the experimental and numerical results. The value used for parameter E in the model is compatible with the previous works in the literature (Biesheuvel et al., 2014; Dykstra et al. 2016a, 2016b; Guyes et al., 2017; Kim et al., 2015a). Fig. 2 depicts the salt adsorption, charge transferred, and charge efficiency of both experimental and numerical data. As it can be seen in this figure, although there is a good agreement between the values obtained from the experiments and the model for the adsorbed salt δ, there is a discrepancy between the experimental and numerical results for the charge transferred q and charge efficiency Λ in cases at a relatively low initial concentration (1 mM). We believe this indicates that there is another resistive mechanism in these systems which has not been included in the model developed here. These cases experience comparably low electrical currents (less than 13 mA) which as discussed by Hemmatifar et al., favor unwanted parasitic energy losses due to Faradaic reactions (Hemmatifar et al., 2016). As mentioned in the Theory section, Faradaic losses are not considered

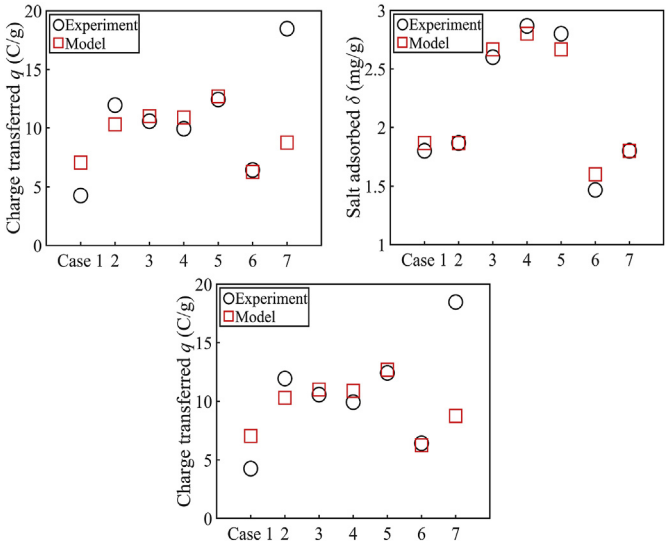

Fig. 2. Experimental and numerical values of the salt adsorption, charge, and charge efficiency of the investigated cases.

in this work and we hypothesize that the difference between the numerical and experimental values of q and Λ in the mentioned cases is caused by neglecting the parasitic losses in the model. We verify this hypothesis by repeating the experiments for Case 1, which shows a somewhat considerable disagreement between the numerical and experimental results, at lower applied voltages. Further discussion on this is provided in the next section.

Next, the temporal effluent concentration profiles of the investigated cases are used to evaluate the macropore to micropore transfer rate constant k. Fig. 3 shows the concentration profile at the exit of each CDI unit over time, normalized by the initial concentration. Electro-sorption resistance between the micro- and macropores is a relatively new concept and has not been fully investigated. Here, based on the obtained numerical and experimental results, we believe it is indeed an important component of the theory describing the transport mechanisms in CDI and one that cannot be neglected. Furthermore, we hypothesize that k is a function of the characteristics of the system. The obtained results here show an inverse relation between k and the Modified Damköhler number Da which is defined as the ratio of the bulk advection and the electro-diffusion time constants. Fig. 4 depicts k versus Da for the analyzed cases. In systems with high $t_{bulk\text{-}adv}$ and relatively low $t_{elec\text{-}diff}$ (high Da), slow advection cannot keep pace with the relatively quick electro-diffusion and is not able to provide ionic species for adsorption at a sufficiently fast rate. This can result in significant local depletion of ions in the macropores, leading to what is known as ion “starvation”. As studied before, in this condition some regions of the electrode locally experience an insufficient number of ions available for electro-adsorption, a phenomenon which limits the motion of the species from the macropores into the micropores and hinders the entire electro-sorption process in the electrodes (Hawks et al., 2018b; Hemmatifar et al., 2015; Porada et al., 2013; Qu et al., 2018; Zhao et al., 2013). This eventually translates into a higher transport resistance from the macropores into the micropores, or in other words, lower values of the transfer rate constant k in the systems. This phenomenon can also be considered similar to the limiting current in an electrochemical cell where the charge transfer process is restricted by the zero concentration at the surface of the electrode and is mass-transfer controlled (Prentice, 1991).

As mentioned earlier, in our previous work we conducted a

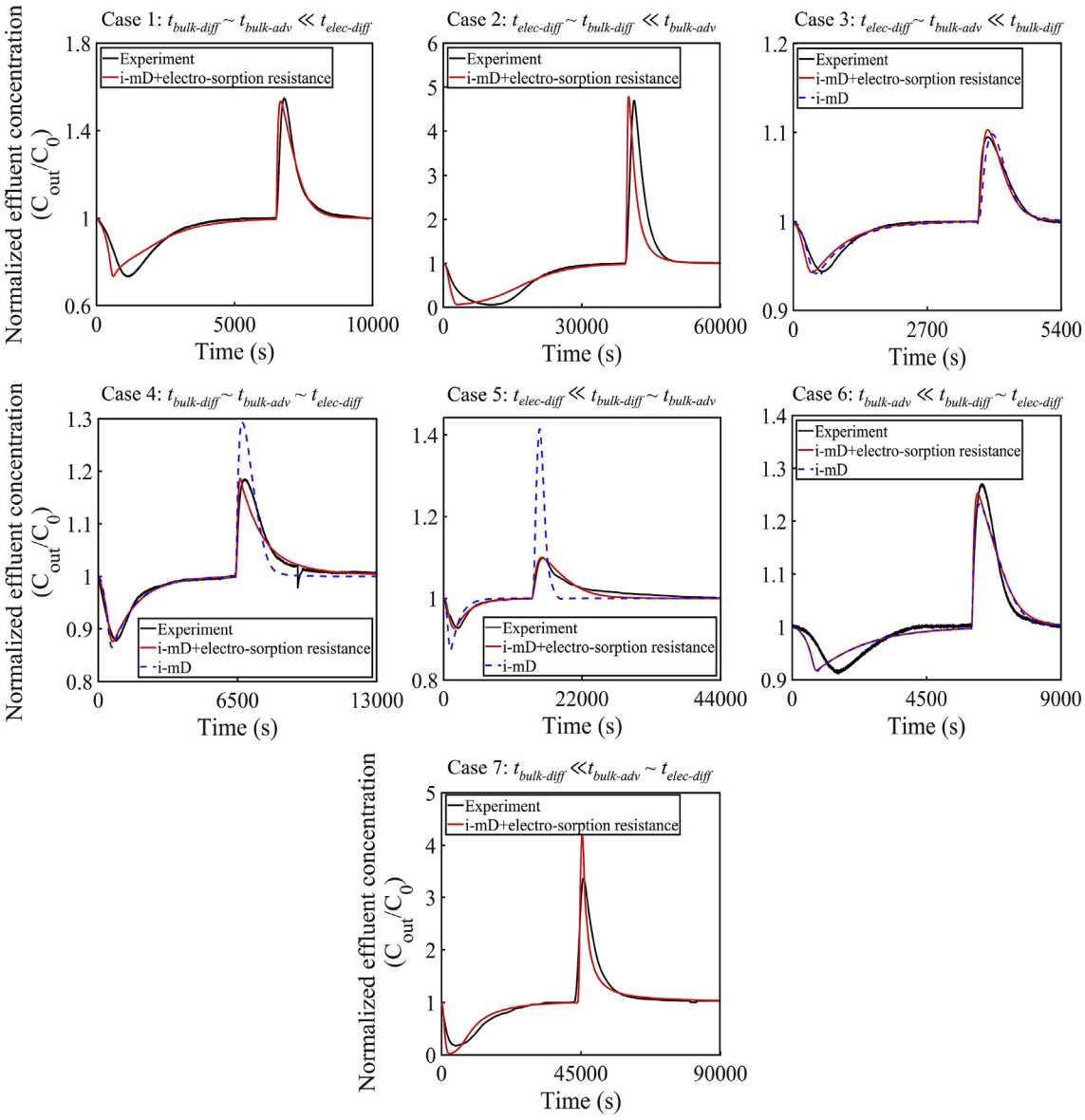

Fig. 3. Experimental and numerical results of the effluent concentration profile of the investigated cases over time, normalized by their initial concentration. Experimental data and the numerical predictions obtained from the model proposed here (non-negligible electro-sorption resistance between the micro- and macropores) and the classic i-mD theory (no electro-sorption resistance) are depicted in black, red, and dashed blue lines, respectively. The classic i-mD model fails to fully predict the effluent concentration profile in Cases 1, 2, and 7 (severe ion starvation). (For interpretation of the references to colour in this figure legend, the reader is referred to the Web version of this article.)

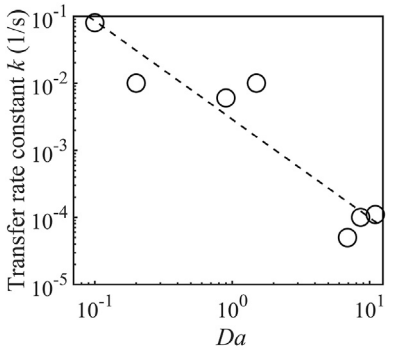

Fig. 4. Transfer rate constant k versus the Modified Damköhler number Da (=$t_{bulk\text{-}adv}$/$t_{elec\text{-}diff}$) for the investigated cases in this work. The data obtained here suggests an inverse relation between the transfer rate constant and the Da number. The dashed line serves to guide the eyes.

parametric study on the transport mechanisms considered in the mD-based models (i.e. bulk advection, bulk diffusion, and the microscale electro-diffusion without electro-sorption resistance) and there we showed that in each system the time at which the effluent concentration reaches its minimum value is in the order of the bulk advection timescale (Salamat and Hidrovo, 2018). Nevertheless, as it was concluded from those results, the interrelation between the transport phenomena of the system determines the total duration of the desalination and regeneration steps, and not a single mechanism. The results here also suggest an inverse relationship between the desalination time t_{desal}, which is the time required for completion of the salt removal (i.e. when the effluent concentration gets back to its initial value), and the transfer rate constant k (see Fig. 5). As this figure shows, in cases with very low rate constant (high electro-sorption resistance), the electro-sorption of the ions into and out of the micropores could be the

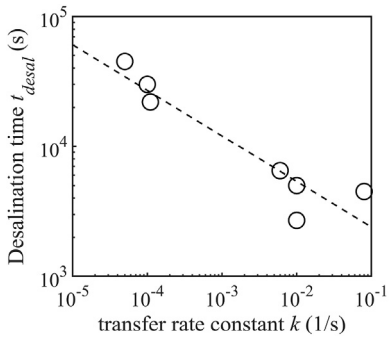

Fig. 5. Desalination time t_{desal} versus the transfer rate constant k of the investigated cases. These data show that there is an inverse relation between the duration of the desalination and the rate constant. In other words, they suggest a direct correlation between the desalination time and the electro-sorption resistance. The dashed line serves to guide the eyes.

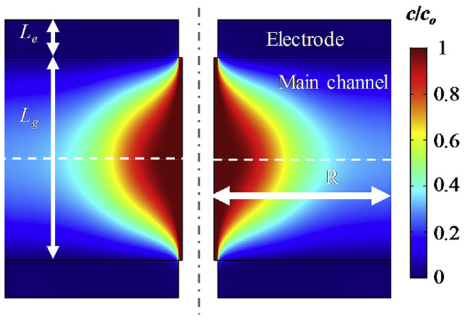

Fig. 6. Normalized concentration in the electrodes' macropores and the main channel (not-to-scale) of the circular fbCDI cell investigated in Case 2 ($c_o = 1$ mM, $Pe_m = 0.1$, $Da = 8.6$, and $Da_{II} = 0.8$), utilizing the classic i-mD theory (no adsorption/desorption resistance between the macro- and micropores). This snapshot is taken at $t = 1010$ s ($\approx 3t_{elec\text{-}diff}$), after which the model fails to model the process due to the severe ion depletion taking place in the macropores. Water enters the main channel via the tube at the center of the cell (not shown here) and radially propagates through the space between the two electrodes (assuming fully developed velocity profile). The white and gray dashed lines show the horizontal and vertical centerlines of the circular cell, respectively. R is the radius of the main channel and L_g and L_e are the gap distance and thickness of the electrodes, respectively.

limiting transport mechanism. In these systems, the ion starvation is so severe that it could dominate the whole desalination step, hindering the completion of the salt adsorption process. Since a somewhat similar trend (inverse relation) is observed between the transfer rate *k* constant and the *Da* number in the cases investigated here (see Fig. 4), we hypothesize that coupled with the other transport mechanisms, the rate limited electro-sorption also determines the overall rate of the salt removal process of each system.

To evaluate the performance of the proposed model in describing the physics of CDI systems, we compare the obtained data with the numerical estimation of the classic i-mD theory where no electro-sorption is included in the model (see Fig. 3). It is worth mentioning that most of the mD-based models developed so far for describing CDI have also demonstrated a good agreement with experimental data, yet these models have not been validated against cases subject to ion starvation (Biesheuvel et al., 2011a; Guyes et al., 2017; Hemmatifar et al., 2015; Porada et al., 2013). The cases studied by these theories mostly have relatively high initial concentrations (>10 mM) and fast flow rates in the main channel. Analyzing and optimizing the water treatment performance of CDI systems at low initial concentrations are equally vital, especially for water softening and heavy metal removal applications (Choi et al., 2019; Huang et al., 2016; Liu et al., 2017).

This comparison is conducted for all the cases investigated here. As it is shown in Fig. 3, in all the cases with low initial concentration (<2 mM) and relatively slow bulk advection, the 2D model without the transport resistance (i.e. the classic i-mD theory) cannot fully capture the dynamics of the process as it encounters convergence complexities. A closer study of these cases reveals that neglecting the rate-limited adsorption/desorption results in local ion depletion zones in the macropores where the concentration reaches values extremely close to zero. Fig. 6 illustrates the normalized concentration in the main channel and electrodes' macropores at $t = 1010$ s of Case 2 which is about three times of the electro-diffusion timescale ($3t_{elec\text{-}diff}$), simulated using the i-mD theory without considering the electro-sorption resistance. In this case, the initial concentration is 1 mM and $Pe_m = 0.1$, $Da = 8.6$, and $Da_{II} = 0.8$. As it can be seen from this figure, most of the macropores in the electrodes are experiencing severe salt starvation and near zero concentration at this instant, after which the model fails to describe the transport mechanisms in the cell. In fact, all the systems with low initial concentration studied here face the same convergence problem where the i-mD model cannot accurately describe the transport mechanisms taking place in the unit (see Fig. S5 for more illustration of the cases with low initial salinity and slow flow rate facing these complications when being simulated with the classic i-mD model).

It should also be noted that although the classic i-mD theory can model CDI systems with higher initial concentrations, it cannot closely predict the performance of the systems with high *Da* number. For example, in Case 5 investigated here ($Da \approx 11$), a substantial discrepancy between the numerical and experimental data is observed when no resistance is assumed for the transport of the ions between the micro- and macropores. As it can be seen from Fig. 3, while the classic i-mD model (no electro-sorption resistance) poorly describes the concentration profile at the exit of this system, the model developed here offers a much more accurate prediction of the experimental data by considering the transport resistance between the micro- and macropores. As mentioned above, in this system, the electro-sorption is the key mechanism limiting the whole desalination performance and omitting this transport resistance from the mathematical model results in inaccurate performance evaluation.

4.2. Performance evaluation

To further analyze the desalination and energetic performance of the investigated cases *UDT*, *ODRP*, and η are calculated for each system and shown in Fig. 7. The obtained results show a good agreement between the numerical and experimental performances. As discussed previously, in the model implemented here, no parasitic reaction losses are being considered and we believe that the current leakage is the main reason for the discrepancy between the experimental and numerical results from the model developed here. To verify this, Case 1 ($Pe_m = 1.7$, $Da = 0.2$, $Da_{II} = 0.3$) which shows a non-negligible disagreement between the experimental and numerical results for q, Λ, and η is repeated at lower external voltages. As shown previously, increasing the applied voltage intensifies the occurrence of the Faradaic reactions (He et al., 2016; Zhang et al., 2018). Consistent with the previous findings, more discrepancy between the experimental and numerical data is also observed here by increasing the external voltage (see section S6 of the Supplementary Information document for the obtained results). This, in fact, demonstrates the robustness of the proposed model in predicting the performance of CDI-based systems, especially in the absence of Faradaic reactions. Although the focus of this study has been on investigating the significance of the electro-sorption resistance, these results underline the importance

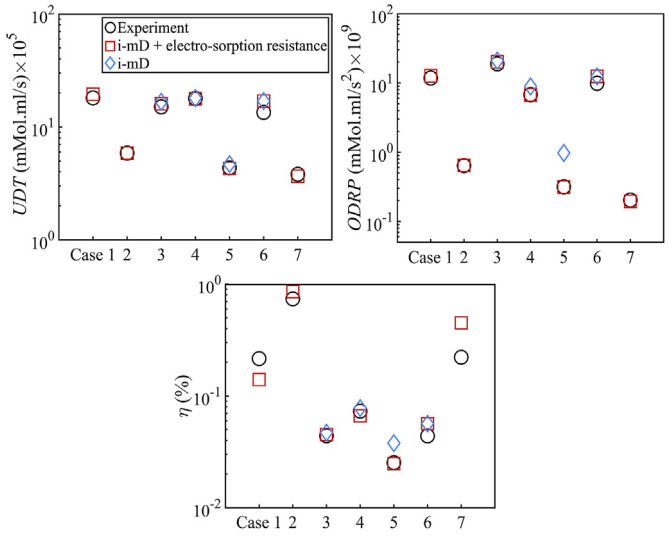

Fig. 7. Values of UDT, ODRP, and η of the investigated cases obtained from the experiments, the model proposed here (i-mD + electro-sorption resistance), and the classic i-mD theory (no electro-sorption resistance). UDT and ODRP refer to the desalination and overall (desalination and regeneration combined) performance, respectively, and η stands for the thermodynamic efficiency. The classic i-mD model, where the micro-macropore transport resistance is not considered, is not able to fully describe transport dynamics in cases 1, 2, and 7 (severe ion starvation).

of integrating Faradaic reactions with the theoretical model in the future studies. We refer the reader to the Supplementary Information document, section S6, for further details on this.

As it can be inferred from Fig. 7, the most noticeable disagreement between the thermodynamic efficiency values obtained from the experimental data and the proposed model can be seen in the cases where the classic i-mD is not able to completely describe the dynamics of the transport in CDI (low initial concentration cases). Although addition of the electro-sorption resistance in the numerical model does not lead to sufficiently accurate estimation of the energetic efficiency of these cases, yet this analysis proves the importance of including all the resistances in a CDI system when assessing its performance compared to other CDI units and even other desalination technologies. Specifically, as these cases offer higher energetic efficiencies, it is necessary to obtain a complete and accurate description of the transport mechanisms for efficiency prediction and optimization purposes. As the recent discussion between Ramachandran et al. and Qin et al. revealed, considering correct electrical, ionic, and transport resistances in CDI is the key element for reaching objective evaluation of the energetic efficiency of this technology compared to other water treatment methods, such as RO (Qin et al., 2019; Qu et al., 2016; Ramachandran et al., 2019a). We believe that by including other resistance mechanisms in the model, such as Faradaic reactions, numerical simulations will achieve a more precise prediction of the CDI systems' performance under various operational conditions.

Another important point which should not be overlooked is that increasing the adsorption capacity of the porous electrodes, for example by increasing the surface area, also further facilitates the occurrence of ion starvation in CDI cells. As the community of CDI aims at improving the efficiency of this system in removing ions by utilizing high capacity electrodes, reaching a robust and high-fidelity mathematical framework which can fully capture this phenomenon is therefore highly crucial.

Furthermore, as it was discussed in the previous section, although the classic i-mD theory can model CDI systems with higher initial concentrations, it cannot correctly predict the performance of the systems with high *Da* number. In case 5, for instance, with slow bulk advection and fast electro-diffusion ($Da \approx 11$) ignoring the rate-limited transfer of the ions between the micro- and macropores leads to a near 50% and 210% error increase in estimating η and *ODRP*, respectively. In this system, the rate-limited transfer of ions between the micro- and macropores is the main mechanism limiting the whole ion removal process. As it can be seen from Fig. 3, neglecting this transport resistance leads to an inaccurate estimation of the desalination and regeneration duration (t_{desal} and t_{regen}), and consequently, to high discrepancy between the experimental and numerical values of the water recovery ratio (*WR*) and the total processing time (t_{total}). These discrepancies eventually translate into an imprecise evaluation of the energetic efficiency (η) and the overall desalination and regeneration performance (*ODRP*) in this system. A detailed error analysis of the classic i-mD theory and the proposed model in predicating the energetic and desalination performance of the studied CDI systems is provided in Table S8 in the Supplementary Information.

Nevertheless, as the results presented in Figs. 3 and 7 demonstrate, ignoring the electro-sorption resistance in the numerical model (the classic i-mD theory) still offers an acceptable performance prediction in cases with low *Da* number. The higher transfer rate constant *k* of these cases, which means faster electro-sorption or, in other words, micro-macropore transfer with less resistance, indicates that the electro-sorption is not the main mechanism limiting the whole ion removal process in these systems and their performance is in fact constrained by the other transport mechanisms.

4.3. Developing versus fully developed systems

As it was numerically discussed in the previous work, whether the CDI unit has a fully-developed or developing convective-diffusive regime highly affects the desalination and energetic performance of the system (Salamat and Hidrovo, 2018). In the former regime, diffusion of the species towards the porous electrodes is faster than their advection in the bulk ($Pe_m < 1$), creating fully-developed convective-diffusive layers. In the latter regime, however, the bulk advection transport of the ions is faster than their bulk diffusion towards the electrode ($Pe_m > 1$), and the diffusion of the species is mainly limited to the thin convective-diffusive layer developing near the interface of the electrodes and the main stream.

The overall performance and thermodynamic efficiency of the conducted experiments versus their Pe_m are shown in Fig. 8. Previous studies discussed the adverse effect of fast advection and slow diffusion in the main channel (high Pe_m) on the effluent concentration reduction percentage (equal to $(c_o - c_{out})/c_o \times 100$) (Mutha et al., 2018; Perez et al., 2013). However, numerical analysis has proved that despite the apparent disadvantage of developing regimes with high Pe_m in decreasing the effluent concentration, their overall desalination performance is better than systems with low Pe_m as higher volumes of water are desalinated in a shorter time (Salamat and Hidrovo, 2018). This suggests that over the same period, water can be processed at a developing regime through a multi-cycle desalination configuration (where at each cycle the effluent of the previous cycle is further desalinated to reach a final desired lower concentration) rather than through one desalination cycle at a fully-developed regime. The experimental results obtained here also demonstrate that CDI units performing in the developing regime offer a better desalination performance as they can desalinate more volumes of the inlet solution in a shorter amount of time, even though they hit a lower desalination percentage per cycle in comparison with the fully-developed systems.

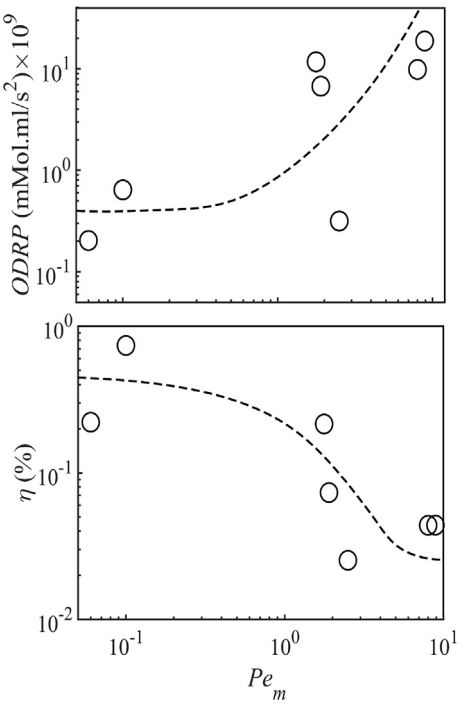

Fig. 8. Experimental values of the overall performance and thermodynamic efficiency versus the mass Péclet number ($=t_{bulk\text{-}diff}/t_{bulk\text{-}adv}$). These results demonstrate the trade-off between the overall desalination and regeneration performance of CDI cells and their energetic efficiency as the mass Péclet number increases. The dashed lines serve to guide the eyes.

In other words, increasing the Pe_m leads to better overall desalination performance. However, as both numerical and experimental data present, fully-developed systems are an energetically better alternative for desalinating a given solution. In fact, due to their higher levels of desalination, fully-developed systems are thermodynamically more efficient. This has also been investigated by Wang et al. where increasing the salinity reduction was recommended for improving the thermodynamic efficiency (Wang et al., 2019).

5. Conclusion

Here, the i-mD approach coupled with Nernst-Planck transport theory was used to model the motion of the ionic species in a CDI unit in two dimensions. The model was further improved by incorporating the transport resistance between the micro- and macropores. To validate the model, desalination cases with different transport timescales were numerically and experimentally investigated. A good agreement between both sets of data was demonstrated and we hypothesized that the transfer rate constant describing the rate-limited transport of the species from the macropores into the micropores depends on the ratio of the bulk advection and microscale electro-diffusion time constants. The desalination and energetic performance of the analyzed systems were also evaluated using inclusive metrics defined in our previous work. The results presented here showed that the model where the rate-limited transfer of the ions between the micro- and macropores is neglected (the classic i-mD) fails to fully describe the transport of the species within the CDI cell in systems at low initial concentrations and high adsorption capacity, while the presented theory closely modeled the dynamics of such cases. Moreover, compared to the classic i-mD theory, the model developed here led to improvement of the desalination performance and energy efficiency estimation by up to 50% and 210%, respectively, in systems at high *Da* number (fast electro-diffusion and slow bulk advection) which are subject to severe ion starvation. Hence, the inclusion of this resistance in CDI theories is of paramount importance for objective and accurate efficiency evaluation of this water desalination method, especially when comparing its performance with other water treatment technologies.

Furthermore, confirming the numerical results, the experimental data indicated that while systems with developing convective-diffusive layers (mass Péclet number > 1) have better desalination performance in terms of the desalination percentage, rate of salt removal, total desalinated volume, and water recovery ratio, they offer an inferior energy efficiency relative to the systems with fully-developed convective-diffusive layers (mass Péclet number < 1). The proposed theoretical framework can be extended beyond CDI systems and can provide critical guidelines for designing effective and efficient water desalination and ion removal systems to meet various application specifications.

Declaration of competing interest

The authors declare that they have no known competing financial interests or personal relationships that could have appeared to influence the work reported in this paper.

Acknowledgment

This work was supported by the United States Bureau of Reclamation (U.S. Department of the Interior, DOI) grant No. R17AC00145.

Appendix A. Supplementary data

Supplementary data to this article can be found online at https://doi.org/10.1016/j.watres.2019.115286.

References

Anderson, M.A., Cudero, A.L., Palma, J., 2010. Capacitive deionization as an electrochemical means of saving energy and delivering clean water. Comparison to present desalination practices: will it compete? Electrochim. Acta 55 (12), 3845–3856.
Arulrajan, A.C., Ramasamy, D.L., Sillanpää, M., van der Wal, A., Biesheuvel, P.M., Porada, S., Dykstra, J.E., 2019. Exceptional water desalination performance with anion-selective electrodes. Adv. Mater. 1806937.
Bejan, A., 2016. Advanced Engineering Thermodynamics. John Wiley & Sons.
Bhat, A.P., Reale, E.R., Cerro, M.d., Smith, K.C., Cusick, R.D., 2019. Reducing impedance to ionic flux in capacitive deionization with Bi-tortuous activated carbon electrodes coated with asymmetrically charged polyelectrolytes. Water Res. X 100027.
Biesheuvel, P., Porada, S., Levi, M., Bazant, M.Z., 2014. Attractive forces in microporous carbon electrodes for capacitive deionization. J. Solid State Electrochem. 18 (5), 1365–1376.
Biesheuvel, P.M., 2009. Thermodynamic cycle analysis for capacitive deionization. J. Colloid Interface Sci. 332 (1), 258–264.
Biesheuvel, P.M., Fu, Y., Bazant, M.Z., 2011a. Diffuse charge and Faradaic reactions in porous electrodes. Physical Review E 83 (6), 061507.
Biesheuvel, P.M., Fu, Y., Bazant, M.Z., 2012. Electrochemistry and capacitive charging of porous electrodes in asymmetric multicomponent electrolytes. Russ. J. Electrochem. 48 (6), 580–592.
Biesheuvel, P.M., Zhao, R., Porada, S., van der Wal, A., 2011b. Theory of membrane capacitive deionization including the effect of the electrode pore space. J. Colloid Interface Sci. 360 (1), 239–248.
Choi, J., Dorji, P., Shon, H.K., Hong, S., 2019. Applications of capacitive deionization: desalination, softening, selective removal, and energy efficiency. Desalination 449, 118–130.
Cohen, I., Avraham, E., Bouhadana, Y., Soffer, A., Aurbach, D., 2015. The effect of the flow-regime, reversal of polarization, and oxygen on the long term stability in capacitive de-ionization processes. Electrochim. Acta 153, 106–114.
Demirer, O.N., Naylor, R.M., Perez, C.A.R., Wilkes, E., Hidrovo, C., 2013. Energetic performance optimization of a capacitive deionization system operating with transient cycles and brackish water. Desalination 314, 130–138.
Dykstra, J.E., Dijkstra, J., van der Wal, A., Hamelers, H.V.M., Porada, S., 2016a. On-line

method to study dynamics of ion adsorption from mixtures of salts in capacitive deionization. Desalination 390, 47–52.
Dykstra, J.E., Keesman, K.J., Biesheuvel, P.M., van der Wal, A., 2017. Theory of pH changes in water desalination by capacitive deionization. Water Res. 119, 178–186.
Dykstra, J.E., Zhao, R., Biesheuvel, P.M., van der Wal, A., 2016b. Resistance identification and rational process design in Capacitive Deionization. Water Res. 88, 358–370.
Elimelech, M., Phillip, W.A., 2011. The future of seawater desalination: energy, technology, and the environment. Science 333 (6043), 712–717.
Gao, X., Omosebi, A., Holubowitch, N., Landon, J., Liu, K., 2017. Capacitive deionization using alternating polarization: effect of surface charge on salt removal. Electrochim. Acta 233, 249–255.
Gao, X., Omosebi, A., Landon, J., Liu, K., 2015. Surface charge enhanced carbon electrodes for stable and efficient capacitive deionization using inverted adsorption-desorption behavior. Energy Environ. Sci. 8 (3), 897–909.
Gao, X., Omosebi, A., Ma, Z., Zhu, F., Landon, J., Ghorbanian, M., Kern, N., Liu, K., 2019. Capacitive deionization using symmetric carbon electrode pairs. Environ. Sci.: Water Res. Technol. 5 (4), 660–671.
Gao, X., Porada, S., Omosebi, A., Liu, K.L., Biesheuvel, P.M., Landon, J., 2016. Complementary surface charge for enhanced capacitive deionization. Water Res. 92, 275–282.
Guyes, E.N., Shocron, A.N., Simanovski, A., Biesheuvel, P.M., Suss, M.E., 2017. A one-dimensional model for water desalination by flow-through electrode capacitive deionization. Desalination 415, 8–13.
Hand, S., Shang, X., Guest, J.S., Smith, K.C., Cusick, R.D., 2019. Global sensitivity analysis to characterize operational limits and prioritize performance goals of capacitive deionization technologies. Environ. Sci. Technol. 53 (7), 3748–3756.
Hatzell, K.B., Hatzell, M.C., Cook, K.M., Boota, M., Housel, G.M., McBride, A., Kumbur, E.C., Gogotsi, Y., 2015. Effect of oxidation of carbon material on suspension electrodes for flow electrode capacitive deionization. Environ. Sci. Technol. 49 (5), 3040–3047.
Hatzell, K.B., Iwama, E., Ferris, A., Daffos, B., Urita, K., Tzedakis, T., Chauvet, F., Taberna, P.-L., Gogotsi, Y., Simon, P., 2014. Capacitive deionization concept based on suspension electrodes without ion exchange membranes. Electrochem. Commun. 43, 18–21.
Hawks, S.A., Knipe, J.M., Campbell, P.G., Loeb, C.K., Hubert, M.A., Santiago, J.G., Stadermann, M., 2018a. Quantifying the flow efficiency in constant-current capacitive deionization. Water Res. 129, 327–336.
Hawks, S.A., Ramachandran, A., Porada, S., Campbell, P.G., Suss, M.E., Biesheuvel, P.M., Santiago, J.G., Stadermann, M., 2018b. Performance metrics for the objective assessment of capacitive deionization systems. Water Res.
Hawks, S.A., Ramachandran, A., Porada, S., Campbell, P.G., Suss, M.E., Biesheuvel, P.M., Santiago, J.G., Stadermann, M., 2019. Performance metrics for the objective assessment of capacitive deionization systems. Water Res. 152, 126–137.
He, D., Wong, C.E., Tang, W., Kovalsky, P., Waite, T.D., 2016. Faradaic reactions in water desalination by batch-mode capacitive deionization. Environ. Sci. Technol. Lett. 3 (5), 222–226.
He, F., Biesheuvel, P.M., Bazant, M.Z., Hatton, T.A., 2018. Theory of water treatment by capacitive deionization with redox active porous electrodes. Water Res. 132, 282–291.
Hemmatifar, A., Oyarzun, D.I., Palko, J.W., Hawks, S.A., Stadermann, M., Santiago, J.G., 2017. Equilibria model for pH variations and ion adsorption in capacitive deionization electrodes. Water Res. 122, 387–397.
Hemmatifar, A., Palko, J.W., Stadermann, M., Santiago, J.G., 2016. Energy breakdown in capacitive deionization. Water Res. 104, 303–311.
Hemmatifar, A., Ramachandran, A., Liu, K., Oyarzun, D.I., Bazant, M.Z., Santiago, J.G., 2018. Thermodynamics of Ion Separation by Electrosorption. 1803.11532.
Hemmatifar, A., Stadermann, M., Santiago, J.G., 2015. Two-dimensional porous electrode model for capacitive deionization. J. Phys. Chem. C 119 (44), 24681–24694.
Huang, Z., Lu, L., Cai, Z., Ren, Z.J., 2016. Individual and competitive removal of heavy metals using capacitive deionization. J. Hazard Mater. 302, 323–331.
Jande, Y.A.C., Kim, W.S., 2013. Desalination using capacitive deionization at constant current. Desalination 329, 29–34.
Kastening, B., Heins, M., 2005. Properties of electrolytes in the micropores of activated carbon. Electrochim. Acta 50 (12), 2487–2498.
Kim, T., Dykstra, J., Porada, S., Van der Wal, A., Yoon, J., Biesheuvel, P., 2015a. Enhanced energy and charge efficiencies by increasing the discharge voltage in capacitive deionization. J. Colloid Interface Sci. 446, 317–326.
Kim, T., Dykstra, J.E., Porada, S., van der Wal, A., Yoon, J., Biesheuvel, P.M., 2015b. Enhanced charge efficiency and reduced energy use in capacitive deionization by increasing the discharge voltage. J. Colloid Interface Sci. 446, 317–326.
Liu, J., Lu, M., Yang, J., Cheng, J., Cai, W., 2015. Capacitive desalination of ZnO/activated carbon asymmetric capacitor and mechanism analysis. Electrochim. Acta 151, 312–318.
Liu, P., Yan, T., Zhang, J., Shi, L., Zhang, D., 2017. Separation and recovery of heavy metal ions and salt ions from wastewater by 3D graphene-based asymmetric electrodes via capacitive deionization. J. Mater. Chem. 5 (28), 14748–14757.
Mubita, T.M., Porada, S., Biesheuvel, P.M., van der Wal, A., Dykstra, J.E., 2018. Capacitive deionization with wire-shaped electrodes. Electrochim. Acta 270, 165–173.
Mutha, H.K., Cho, H.J., Hashempour, M., Wardle, B.L., Thompson, C.V., Wang, E.N., 2018. Salt rejection in flow-between capacitive deionization devices. Desalination 437, 154–163.
Newman, J., Thomas-Alyea, K.E., 2012. Electrochemical Systems. John Wiley & Sons.
Omosebi, A., Gao, X., Holubowitch, N., Li, Z., Landon, J., Liu, K., 2017. Anion exchange membrane capacitive deionization cells. J. Electrochem. Soc. 164 (9), E242–E247.
Omosebi, A., Gao, X., Landon, J., Liu, K., 2014. Asymmetric electrode configuration for enhanced membrane capacitive deionization. ACS Appl. Mater. Interfaces 6 (15), 12640–12649.
Oren, Y., 2008. Capacitive deionization (CDI) for desalination and water treatment — past, present and future (a review). Desalination 228 (1–3), 10–29.
Oyarzun, D.I., Hemmatifar, A., Palko, J.W., Stadermann, M., Santiago, J.G., 2018. Adsorption and capacitive regeneration of nitrate using inverted capacitive deionization with surfactant functionalized carbon electrodes. Separ. Purif. Technol. 194, 410–415.
Perez, C.A.R., Demirer, O.N., Clifton, R.L., Naylor, R.M., Hidrovo, C.H., 2013. Macro analysis of the electro-adsorption process in low concentration NaCl solutions for water desalination applications. J. Electrochem. Soc. 160 (3), E13–E21.
Porada, S., Borchardt, L., Oschatz, M., Bryjak, M., Atchison, J.S., Keesman, K.J., Kaskel, S., Biesheuvel, P.M., Presser, V., 2013. Direct prediction of the desalination performance of porous carbon electrodes for capacitive deionization. Energy Environ. Sci. 6 (12), 3700–3712.
Prentice, G., 1991. Electrochemical Engineering Principles.
Qin, M., Deshmukh, A., Epsztein, R., Patel, S.K., Owoseni, O.M., Walker, W.S., Elimelech, M., 2019. Comparison of energy consumption in desalination by capacitive deionization and reverse osmosis. Desalination 455, 100–114.
Qu, Y., Campbell, P.G., Gu, L., Knipe, J.M., Dzenitis, E., Santiago, J.G., Stadermann, M., 2016. Energy consumption analysis of constant voltage and constant current operations in capacitive deionization. Desalination 400, 18–24.
Qu, Y., Campbell, P.G., Hemmatifar, A., Knipe, J.M., Loeb, C.K., Reidy, J.J., Hubert, M.A., Stadermann, M., Santiago, J.G., 2018. Charging and transport dynamics of a flow-through electrode capacitive deionization system. J. Phys. Chem. B 122 (1), 240–249.
Ramachandran, A., Hemmatifar, A., Hawks, S.A., Stadermann, M., Santiago, J.G., 2018. Self similarities in desalination dynamics and performance using capacitive deionization. Water Res. 140, 323–334.
Ramachandran, A., Oyarzun, D.I., Hawks, S.A., Campbell, P.G., Stadermann, M., Santiago, J.G., 2019a. Comments on “Comparison of energy consumption in desalination by capacitive deionization and reverse osmosis”. Desalination 461, 30–36.
Ramachandran, A., Oyarzun, D.I., Hawks, S.A., Stadermann, M., Santiago, J.G., 2019b. High water recovery and improved thermodynamic efficiency for capacitive deionization using variable flowrate operation. Water Res.
Salamat, Y., Hidrovo, C.H., 2018. A parametric study of multiscale transport phenomena and performance characteristics of capacitive deionization systems. Desalination 438, 24–36.
Salamat, Y., Rios Perez, C.A., Hidrovo, C., 2016a. Performance characterization of a capacitive deionization water desalination system with an intermediate solution and low salinity water. J. Energy Resour. Technol. 138 (3), 032003-032003.
Salamat, Y., Rios Perez, C.A., Hidrovo, C., 2016b. Performance improvement of capacitive deionization for water desalination using a multistep buffered approach. J. Energy Resour. Technol. 139 (3), 032003-032003-032006.
Shang, X., Cusick, R.D., Smith, K.C., 2017. A combined modeling and experimental study assessing the impact of fluid pulsation on charge and energy efficiency in capacitive deionization. J. Electrochem. Soc. 164 (14), E536–E547.
Smith, K.C., Dmello, R., 2016. Na-ion desalination (NID) enabled by Na-blocking membranes and symmetric Na-intercalation: porous-electrode modeling. J. Electrochem. Soc. 163 (3), A530–A539.
Stanton, J.S., Anning, D.W., Brown, C.J., Moore, R.B., McGuire, V.L., Qi, S.L., Harris, A.C., Dennehy, K.F., McMahon, P.B., D.,J.R., Böhlke, J.K., 2017. Brackish Groundwater in the United States. U.S. Geological Survey, Reston, VA, p. 185.
Suss, M., Porada, S., Sun, X., Biesheuvel, M., Yoon, J., Presser, V., 2015. Water desalination via capacitive deionization: what is it and what can we expect from it? Energy Environ. Sci.
Suss, M.E., Biesheuvel, P.M., Baumann, T.F., Stadermann, M., Santiago, J.G., 2014. In situ spatially and temporally resolved measurements of salt concentration between charging porous electrodes for desalination by capacitive deionization. Environ. Sci. Technol. 48 (3), 2008–2015.
Tang, W., Liang, J., He, D., Gong, J., Tang, L., Liu, Z., Wang, D., Zeng, G., 2019. Various cell architectures of capacitive deionization: recent advances and future trends. Water Res. 150, 225–251.
Wang, L., Dykstra, J., Lin, S., 2019. Energy efficiency of capacitive deionization. Environ. Sci. Technol.
Wu, T., Wang, G., Dong, Q., Qian, B., Meng, Y., Qiu, J., 2015. Asymmetric capacitive deionization utilizing nitric acid treated activated carbon fiber as the cathode, 176, 426–433.
Xu, P., Drewes, J.E., Heil, D., Wang, G., 2008. Treatment of brackish produced water using carbon aerogel-based capacitive deionization technology. Water Res. 42 (10–11), 2605–2617.
Zhang, C., He, D., Ma, J., Tang, W., Waite, T.D., 2018. Faradaic reactions in capacitive deionization (CDI) - problems and possibilities: a review. Water Res. 128, 314–330.
Zhao, R., Satpradit, O., Rijnaarts, H.H.M., Biesheuvel, P.M., van der Wal, A., 2013. Optimization of salt adsorption rate in membrane capacitive deionization. Water Res. 47 (5), 1941–1952.